# Local contractions regulate E-cadherin rigidity sensing

Yi-An Yang, Emmanuelle Nguyen, Gautham Hari Narayana Sankara Narayana, Melina Heuzé, Chaoyu Fu, Hanry Yu, René-Marc Mège, Benoit Ladoux, Michael Sheetz

CELL BIOLOGY

# Local contractions regulate E-cadherin rigidity sensing

Yi-An Yang[1], Emmanuelle Nguyen[1], Gautham Hari Narayana Sankara Narayana[2], Melina Heuzé[2], Chaoyu Fu[1], Hanry Yu[1,3,4,5], René-Marc Mège[2], Benoit Ladoux[1,2]*, Michael P. Sheetz[1,6,7]*†



**E-cadherin is a major cell-cell adhesion molecule involved in mechanotransduction at cell-cell contacts in tissues. Because epithelial cells respond to rigidity and tension in tissue through E-cadherin, there must be active processes that test and respond to the mechanical properties of these adhesive contacts. Using submicrometer, E-cadherin–coated polydimethylsiloxane pillars, we find that cells generate local contractions between E-cadherin adhesions and pull to a constant distance for a constant duration, irrespective of pillar rigidity. These cadherin contractions require nonmuscle myosin IIB, tropomyosin 2.1, α-catenin, and binding of vinculin to α-catenin. Cells spread to different areas on soft and rigid surfaces with contractions, but spread equally on soft and rigid without. We further observe that cadherin contractions enable cells to test myosin IIA–mediated tension of neighboring cells and sort out myosin IIA–depleted cells. Thus, we suggest that epithelial cells test and respond to the mechanical characteristics of neighboring cells through cadherin contractions.**

## INTRODUCTION

For the proper organization of tissues, cells need to probe the mechanical properties of their microenvironment including both extracellular matrix and neighboring cells through adhesive contacts. These mechanical properties are then transduced into biochemical information to regulate cell functions (*1*), including single and collective cell motility (*2*, *3*), proliferation (*4*), or differentiation (*5*). Of the many mechanical properties that cells control, stiffness appears to be an important parameter that is distinctive for a tissue and is reflected in the cells that constitute the tissue (*6*). It follows that cells should be able to measure the stiffness of their neighbors to enable them to regulate their cell-cell contacts and cytoskeletal rigidity and to organize cell monolayers. Thus, it is important to understand how E-cadherin rigidity might be sensed. Recent studies have found that epithelial cells spread to larger areas on rigid cadherin-coated surfaces than soft (*7*). The testing of cadherin adhesion rigidity (*8*) appears to share similarities with the testing of matrix rigidity described for fibroblasts (*9*). In the context of epithelial cell dynamics, this mechanism may allow cells to adapt to changes in the local stiffness of their neighbors due to cytoskeleton remodeling and reinforcement (*10*–*12*).

Cadherin rigidity is a complex mechanical parameter because it is defined as the force per unit area needed to displace a cadherin adhesion by a given distance. In the case of matrix rigidity sensing, cells pull matrix contacts to a constant deflection and measure the force generated (*13*–*15*). The local matrix rigidity sensor is a sarcomere-like contraction complex (2 μm in length) that contracts matrix adhesions by ~120 nm, and if the force exceeds 25 pN, then a rigid-matrix signal is activated in the cell. The contractions are controlled by receptor tyrosine kinases in terms of the magnitude of deflection, the duration, and the activation of the contractions (*16*, *17*). The sarcomere-like contraction system consists of antiparallel actin filaments anchored by α-actinin, a bipolar myosin filament, and a number of actin-binding proteins including tropomyosin (Tpm) 2.1 (*14*, *15*). Although there are many obvious differences between cadherin and integrin adhesions (*18*), a similar mechanism may be used to sense the rigidity of the E-cadherin contacts, i.e., neighboring cells.

Integrin and cadherin adhesions have many features in common, including that adhesions are built upon distinct nanometer-sized clusters of adhesion molecules (*19*, *20*) and are linked to many actin-binding proteins (*18*). In tissues, cadherin clusters form homophilic interactions that maintain adhesions between cells (*21*) helping to hold the tissue together. As primary components of adhesive contacts, cadherins are major parts of the mechanotransducing systems between cells (*22*, *23*) and are important for tissue morphology (*24*). Many cytoplasmic proteins link these adhesions to the cytoskeleton and provide mechanical continuity across the cell through a dynamic actomyosin network and other filamentous elements (*25*). In addition, a "sarcomeric belt" structure is present at apical cell-cell boundaries of epithelial cells, with nonmuscle myosin II–mediated actomyosin structures interpolated in between cell-cell adhesive complexes at a constant spacing (*26*, *27*). Other mechanical activities of epithelial monolayers also appear to involve actin and myosin contractions of the cadherin adhesions including the formation of cell-cell contacts (*28*), the contraction and bending of cell monolayers (*27*, *29*), and tissue extension. The cadherin adhesion complexes are consequently a major element in mechanosensing events that ultimately shape the tissue and are involved in rigidity sensing and many other processes.

Previous studies have shown that cells generated high forces on large N-cadherin–coated pillars through cellular level contractions that are similar but not identical to matrix traction forces (*8*, *30*). N-cadherin junctions that form on N-cadherin–coated pillar surfaces resemble the morphology and dynamics of native epithelial cell-cell junctions (*8*). Moreover, substrate stiffness modulates the level of force on E-cadherin adhesions that correlates with changes in cell spread area (*7*). If the cadherin-based rigidity-sensing module is similar to the integrin-based sensor, then it should be evident in the deflection patterns of submicrometer diameter pillars (*9*). When we

[1]Mechanobiology Institute, National University of Singapore, Singapore 117411, Singapore. [2]Université de Paris, CNRS, Institut Jacques Monod, F-75013 Paris, France. [3]Department of Physiology, Institute for Digital Medicine (WisDM), Yong Loo Lin School of Medicine, Singapore 117593, Singapore. [4]Institute of Bioengineering and Bioimaging, A*STAR, Singapore 138669, Singapore. [5]CAMP, Singapore-MIT Alliance for Research and Technology, Singapore 138602, Singapore. [6]Department of Biological Sciences, Columbia University, New York, NY 10027, USA. [7]Department of Biochemistry and Molecular Biology, University of Texas Medical Branch, Galveston, TX 77555, USA.
*Corresponding author. Email: misheetz@utmb.edu (M.P.S.); benoit.ladoux@ijm.fr (B.L.)
†Lead contact: misheetz@utmb.edu

placed E-cadherin–expressing cells on submicrometer E-cadherin pillars, we observed local contractile units of 1.2 to 2.4 μm that pulled E-cadherin junctions together to a constant distance of 130 nm, independent of rigidity over a 20-fold range. Unlike the integrin-based contractions, E-cadherin contractions did not require myosin IIA but were rather dependent on myosin IIB, α-catenin, and vinculin and also involved Tpm2.1. When the contractions were depleted, cells spread equally on rigid and soft cadherin, and there was improper sorting of mixed monolayers. The density of cadherin contractions (CCs) correlated with the area of cells on cadherin surfaces, which was consistent with the increased spreading of Madin-Darby canine kidney (MDCK) cells and MCF-10A cells on stiffer E-cadherin surfaces. Thus, it seems that cells create local contraction units between E-cadherin contacts to test mechanical properties of neighboring cells for proper organization of epithelial monolayers.

## RESULTS

### COS-7 and MDCK cells form contractile units on E-cadherin–coated pillars

Previous studies indicated that cadherin adhesion clusters were constantly spaced (*28*, *31*), and E-cadherin clusters were spaced at a distance of ~1.4 μm (*28*). On the basis of those observations, we prepared pillar substrates with a diameter of 600 nm and 1.2-μm center-to-center spacing. When pillars were coated with E-cadherin, cells attached and developed force on the pillars (fig. S1A). To characterize E-cadherin–dependent force generation, we used COS-7 cells, an SV-40–transformed derivative of African green monkey kidney fibroblasts, and MDCK epithelial cells. COS-7 cells were of particular interest because these fibroblast-like cells expressed E-cadherin (*32*) while lacking a major myosin II isoform, myosin IIA (*33*), that was needed to produce local contractions on fibronectin matrices (*17*). Unexpectedly, COS-7 cells were able to adhere to, spread on, and pull E-cadherin pillars and generated local contractions (Fig. 1A, left). The spreading and force generation were similar to earlier studies using large cadherin-coated pillars (*8*, *34*); however, unlike the case with cells on the larger cadherin pillars, these submicrometer pillars revealed local contraction units of 1 to 2 μm like those previously found for integrin-based adhesions (*9*). The criteria for the local contractions were that pairs of pillars moved toward each other for a limited period, and maximum displacements occurred at approximately the same time point (see description below). When COS-7 cells spread on E-cadherin–coated pillars, there were many examples of local contractions (Fig. 1A, right), which were not observed with larger pillars before, indicating that these smaller pillars were able to reveal local contractions in addition to the radial contractions.

In general, it was difficult to separate all local contractile units from radial contractions because multiple contractile units often overlapped, resulting in complex pillar displacements. Although some local contractions were not recorded, we used the very stringent requirement for pairs that two pillars move toward each other and relax at the same time. The computer identification of pillar pairs involved two major criteria: (i) two pillars moved toward each other with their deflections greater than half value of the average maximum deflection for a duration more than 8 s, and (ii) the maximum deflections of both pillars occurred within 5 s time window. We then characterized paired contractions of pillars by two parameters: $D_{max}$, the maximum pillar deflection value from the original position, and

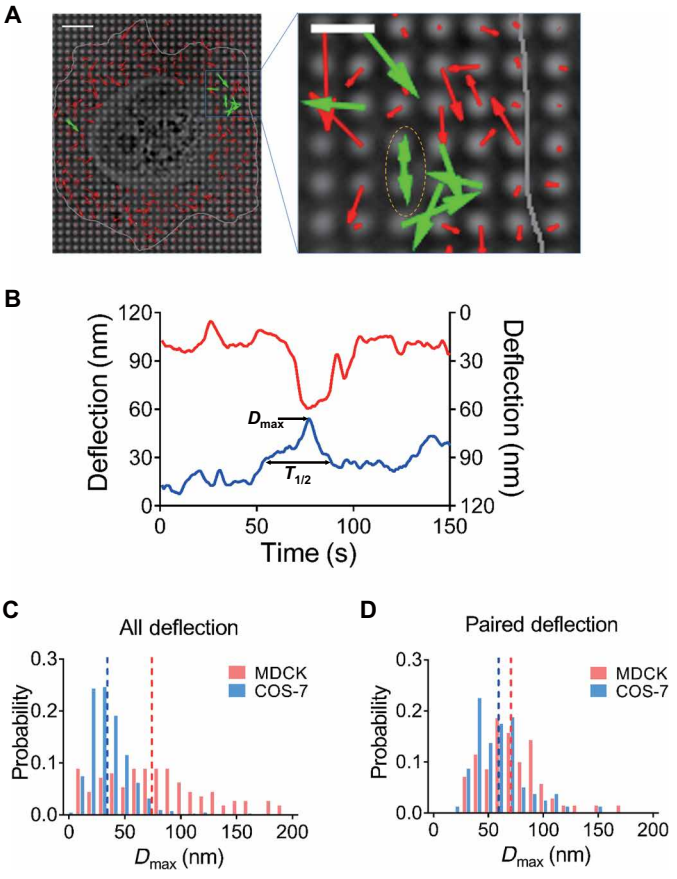


**Fig. 1. Cell generates local contractile units on E-cadherin–coated pillars.** (**A**) Left: Pillar deflection vector map under a COS-7 cell. Red vectors indicate non-paired deflections, green vectors indicate paired deflections, and gray line indicates cell boundary. Scale bar, 5 μm. Right: Amplification of contraction-generation cell spreading area. (**B**) Deflection plot of paired pillars under one contraction event, correlated with pillars indicated in (A) in yellow dashed ellipse. (**C**) Histogram plots of total $D_{max}$ distribution of MDCK cells were higher than those of COS-7 cells, and dashed lines show mean $D_{max}$ value of MDCK and COS-7 cells in respective color. For MDCK cells, $D_{max} = 76.92 \pm 4.332$ nm, $n = 112$ from five cells in two experiments; for COS-7 cells, $D_{max} = 35.7 \pm 0.7837$ nm, $n = 661$ from nine cells from two experiments. (**D**) Histogram plots of $D_{max}$ distribution of paired deflecting pillars in MDCK and COS-7 cells are similar. For MDCK cells, $D_{max} = 71.1 \pm 3.268$ nm, $n = 70$ from five cells in two experiments; for COS-7 cells, $59.65 \pm 2.678$ nm, $n = 80$ from nine cells from two experiments.

$T_{1/2}$, half-peak contraction time that was the length of time that the pillar was pulled farther than half of the $D_{max}$ value in a single pulling event (indicated in Fig. 1B). After analyzing the time course of pillar movements under spreading cells for ~30 min, there was a substantial density of local contractile units, in which pillars deflected and relaxed in a synchronized manner (Fig. 1B; local contractions were noted by dotted line circled pillars in Fig. 1A). Characterization of the contractile units provided a quantitative analysis of the local contractions (more than 2000 contractile pairs were identified in more than 50 cells), and we designated those paired E-cadherin adhesion–dependent contractile events as CCs. Thus, the CCs were substantial in density and were distinct from other pillar displacements.

To determine whether CCs were present in other cells, we chose MDCK epithelial cells. After spreading on E-cadherin pillars for

3 hours, they generated CCs in a similar fashion to COS-7 cells (fig. S1B). Analysis of the $D_{max}$ of all pillar deflections showed that overall contractility was much greater with MDCK cells than with COS-7 cells because of the presence of myosin IIA in MDCK cells (Fig. 1C), while the magnitude of CC deflection was closer between both cell lines (Fig. 1D). These results supported the idea that CCs were generated in a similar fashion and were a common activity across different cell types in contrast to variations in overall force generation. Furthermore, analyses of the pillar deflections showed that the velocities of contraction and relaxation were similar in CCs (fig. S1C), whereas the contraction velocities were significantly higher than relaxation velocities for overall contractions in both MDCK and COS-7 cells (fig. S1D). We also suggest that the CC pairs were unlike integrin-dependent contractions because they formed in the absence of myosin IIA in COS-7 cells. In contrast, large contractions were much less frequent in overall deflections of COS-7 cells, indicating that large contractions observed in overall displacements by MDCK cells were powered by myosin IIA.

Because the local CCs were distinct and highly regular in terms of both $D_{max}$ and duration of contractions, we quantified the CC parameters under a variety of conditions, including different pillar rigidities. When MDCK cells were spread on pillars with different rigidities due to their different heights, the local CCs had very similar $D_{max}$ values (71.1 ± 3.27 nm on 0.75-μm high pillars and 66.9 ± 2.81 nm on 1.5-μm high pillars that had spring constants of 95 and 12 pN/nm, respectively; fig. S2A), indicating that contraction distance was rigidity independent, which was similar to previous observation in local matrix contractions (*14*, *15*). Similar feature was also observed for CCs generated by COS-7 cells spreading on E-cadherin pillars ($D_{max}$ of 59.6 ± 2.68 nm on 0.75-μm high pillars and of 60.9 ± 1.19 nm on 2-μm high pillars that had spring constants of 95 and 5 pN/nm) (fig. S2B). Furthermore, the average $T_{1/2}$ values were about 20.0 s for both COS-7 and MDCK cells (fig. S3A). These results further reinforced the idea that paired contractions were powered by the same process in MDCK and COS-7 cells. Together, both MDCK and COS-7 cells produced CCs that were rigidity independent and had similar $D_{max}$ and $T_{1/2}$ values. Thus, both MDCK and COS-7 cells pulled to a constant deflection on E-cadherin, and then the force of the contractions was proportional to the rigidity.

## E-cadherin–mediated rigidity response correlates with CC density

In previous studies of cell spreading on matrix, rigidity of the matrix was indicative of the density of contractile units and the cell spreading area (*14*, *17*). We then tested whether there was a similar correlation between CC density and spread area on E-cadherin–coated substrata. CC density was measured as the average number of CCs generated by a spreading part of cell during 10 min in a constant area (36 μm$^2$, which is the area of 25 pillars). When MDCK cells spread on soft and stiff polydimethylsiloxane (PDMS) surfaces coated with E-cadherin, the final spread area was larger on stiff (~2 MPa) than on soft gels (~5 kPa) (Fig. 2A). As predicted from the local matrix contractions, the CC density was lower on the soft than on the rigid pillars (Fig. 2B), which correlated with the lower spread area on soft pillars (Fig. 2C). Similarly, the human breast epithelial cells, MCF-10A, also generated more CCs on rigid E-cadherin–coated pillars (Fig. 2D) and spread to larger areas (Fig. 2E), indicating that the correlation between CC generation and spreading exists in different epithelial cell lines.

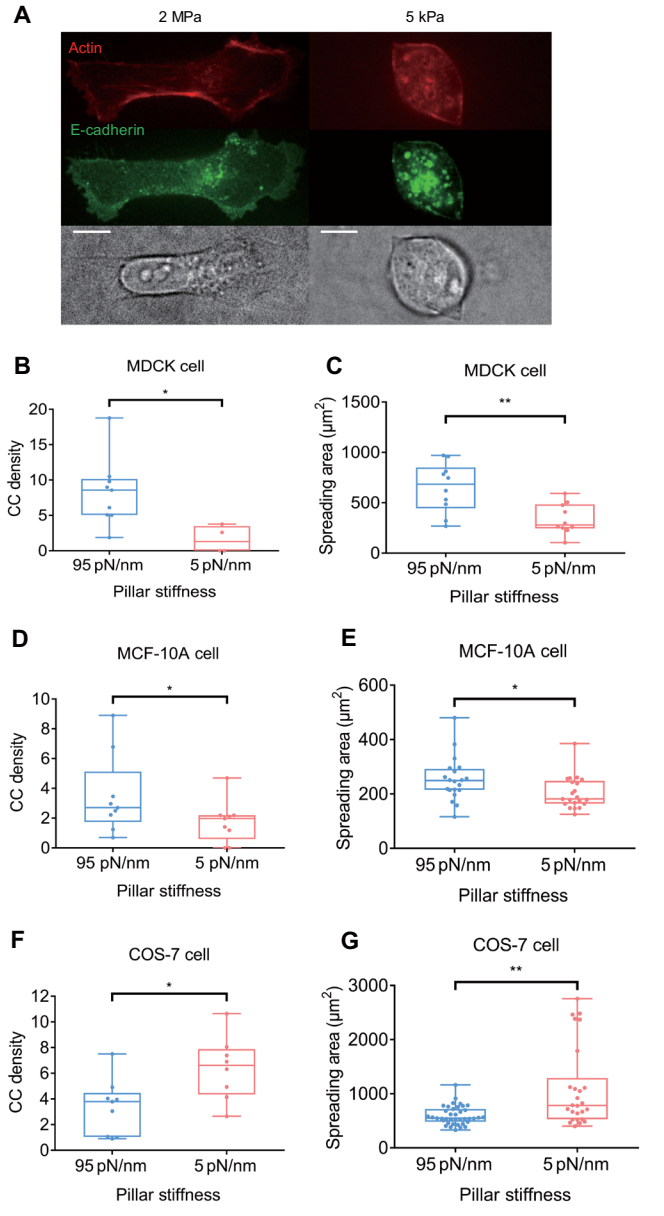


**Fig. 2. CC density correlates with cell spreading area on E-cadherin.** (**A**) On E-cadherin–coated PDMS gel, MDCK cells spread more on stiff 2-MPa gel (left panels) than on soft 5-kPa gel (right panels). Scale bars, 10 μm. (**B**) CC density is higher when MDCK cells spread and pull on stiffer (95 pN/nm) pillars (8.31 ± 1.60 μm$^2$, $n = 9$ spreading events from six cells in four experiments) than on softer (5 pN/nm) pillars (1.60 ± 0.95 μm$^2$, $n = 4$ spreading events from two cells in two experiments). (**C**) MDCK cells spread more on stiffer pillars (650.1 ± 78.1 μm$^2$, $n = 10$ cells in two experiments) than on softer pillars (338.8 ± 47.8 μm$^2$, $n = 10$ cells in two experiments). (**D**) CC density is higher when MCF-10A cells spread on and pull stiffer pillars (3.50 ± 0.89 μm$^2$, $n = 9$ spreading events from five cells in three experiments) than on softer pillars (1.76 ± 0.47 μm$^2$, $n = 9$ spreading events from six cells in two experiments). (**E**) MCF-10A cells spread more on stiffer pillars (254.0 ± 18.0 μm$^2$, $n = 20$ cells in three experiments) than on softer pillars (203.7 ± 12.9 μm$^2$, $n = 21$ cells in two experiments). (**F**) Density of CC generated by COS-7 cells is higher on softer pillars (6.38 ± 0.88 μm$^2$, $n = 8$ spreading events in four cells in two experiments) than on stiffer pillars (3.36 ± 0.72 μm$^2$, $n = 9$ spreading events in four cells in two experiments). (**G**) COS-7 cells spread more on softer pillars (1106.1 ± 147.4 μm$^2$, $n = 26$ cells in two experiments) than on stiffer pillars (598.1 ± 27.5 μm$^2$, $n = 39$ cells in two experiments). *$P < 0.05$; **$P < 0.01$; data are presented as means ± SEM.

However, the density of COS-7 CCs increased on the soft pillars (Fig. 2F). This unexpected result stimulated us to examine the spreading of COS-7 cells on rigid and soft cadherin-coated surfaces. We observed that COS-7 cells spread to a larger area on soft (~5 pN/nm) than on rigid (~95 pN/nm) pillars (Fig. 2G), which correlated with higher CC density on soft pillars. These results indicated that CC formation was rigidity sensitive and promoted cell spreading. However, COS-7 cells, which are transformed cells, did not respond to rigid cadherin in the same way as MDCK cells or MCF-10A cells. COS-7 cells also present abnormal mechanosensing on fibronectin substrates. They spread and grew equally well on soft and rigid fibronectin substrates (*35*). Thus, the general rigidity-sensing (cell-matrix and cell-cell) and rigidity responses of these cells may be altered, leading to a different response of COS-7 cells to CC generation compared to MDCK and MCF-10A cells. In addition, the different responses in stiffness sensing between COS-7 and the other cell types may also be explained by various relative cell-to-substrate stiffness ratios (*36*). COS-7 cells that do not express myosin IIA may be softer than MDCK or MCF-10A cells, leading to different responses within a similar range of stiffnesses.

### α-Catenin and vinculin cooperatively regulate CC

To further investigate the role of cadherin adhesion proteins in CCs, we examined involvement of the major actin-binding proteins in the E-cadherin adhesions, α-catenin and vinculin. Previous studies showed that α-catenin was under force in the cadherin adhesion (*37*) and potentially acted as a molecular mechanosensitive switch (*38*). There was also evidence for involvement of vinculin in linking E-cadherin adhesion complexes to actin (*39*) that was consistent with its role as a force transducer. When α-catenin knockdown (KD) MDCK cells were placed on E-cadherin–coated pillars, CC density was greatly reduced (Fig. 3A). After α-catenin was restored in the KD MDCK cells, a normal level of CCs was observed (Fig. 3B, paired CCs marked by green vectors), showing that α-catenin was critical in forming CCs (Fig. 3C). In addition, we also found that α-catenin KD reduced $T_{1/2}$ value and $D_{max}$ of the overall contractions, which was restored through α-catenin rescue (fig. S3, B and C). These results indicated that α-catenin was a crucial component in CCs and was generally involved in linking cadherin adhesions to the contractile cytoskeleton.

We next tested whether the association of vinculin with α-catenin was important. Although vinculin's role in regulating force generation remained unclear, the interaction between vinculin and α-catenin depended upon the unfolding of α-catenin (*38*, *40*). To test whether α-catenin–vinculin binding affinity affected CC, we rescued α-catenin KD MDCK cells with an α-catenin mutant L344P that did not bind vinculin (*41*). Upon L344P mutant rescue, local CC density and contraction duration remained significantly reduced compared with wild-type (WT) cells (Fig. 3C and fig. S4, A and E). However, contractile force generation was restored in magnitude (fig. S4F). Thus, the interaction between vinculin and α-catenin was important for CC formation.

To determine whether vinculin was also involved in CC formation, we tested vinculin-depleted MDCK cells and characterized their CCs on pillars. We found that vinculin KD cells had a much lower density of CCs when compared with WT MDCK cells, while reexpression of vinculin restored CC density to normal levels (Fig. 3D and fig. S4, B and C). Unexpectedly, vinculin KD in MDCK cells did not decrease overall contractions (fig. S4D), which resembled

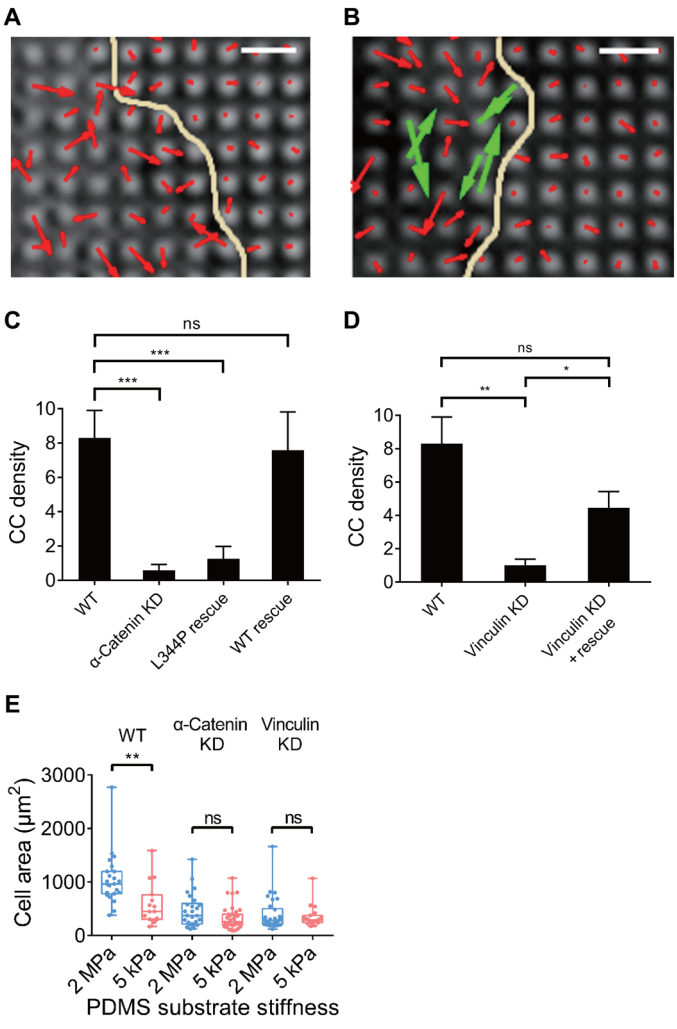


**Fig. 3. Depletion of α-catenin and vinculin in MDCK cells alters CC generation.** Pillar deflection vector maps show that α-catenin KD MDCK cells fail to generate CC (**A**) (red vectors indicate noncontractile deflections), while α-catenin rescue restores CC in KD cells (**B**) (CC in green vectors). Patel yellow line indicates cell boundary. Scale bars, 2 μm. (**C**) Quantification of CC density indicates that MDCK cells suffer from decreased CC density upon α-catenin KD (0.59 ± 0.34, $n = 9$ spreading events from four cells in two experiments) compared with WT MDCK cells (8.31 ± 1.60, $n = 9$ spreading events from six cells in four experiments), while L344P mutated α-catenin fails to restore CC (1.26 ± 0.71, $n = 6$ spreading events from three cells in two experiments), and WT α-catenin restores CC to normal density level (7.59 ± 2.23, $n = 4$ spreading events from two cells in two experiments). (**D**) Vinculin KD decreases CC density in MDCK cells (1.02 ± 0.36, $n = 4$ spreading events from four cells in two experiments) compared with WT MDCK cells (8.31 ± 1.60, $n = 9$ spreading events from six cells in four experiments), while vinculin rescue on KD background restores CC density (4.45 ± 0.97, $n = 6$ spreading events from two cells in one experiment). (**E**) MDCK cells spread into larger areas on 2-MPa E-cadherin–coated gels (1049.4 ± 99.9 μm$^2$, $n = 23$ cells from two experiments) than on 5-kPa gels (591.4 ± 101.0 μm$^2$, $n = 15$ cells from two experiments), while α-catenin KD diminishes such rigidity dependence (464.8 ± 61.8 μm$^2$ on 2-MPa gel, $n = 26$ cells from two experiments; 338.8 ± 38.1 μm$^2$ on 5-kPa gel, $n = 35$ cells from two experiments), so is vinculin KD (392.6 ± 57.1 μm$^2$ on 2-MPa gel, $n = 30$ cells from two experiments; 350.9 ± 46.2 μm$^2$ on 5-kPa gel, $n = 19$ cells from two experiments). ns, nonsignificant; *$P < 0.05$; **$P < 0.01$; ***$P < 0.001$; data are presented as means ± SEM.

the effect of L344P mutant rescue upon α-catenin KD that disabled vinculin binding to α-catenin (fig. S4F). Thus, vinculin was critically involved in the CC mechanism, although vinculin depletion had no significant effect on overall cell contractility.

To further investigate the role of CC activity of MDCK cells in cell spreading, WT cells as well as α-catenin– or vinculin-depleted cells were spread on soft and rigid E-cadherin surfaces. We observed that WT MDCK cells spread more on rigid than on soft substrates, in agreement with previous results on pillars with varying stiffness (Figs. 2D and 3E). When cells lost the ability to form CCs due to α-catenin or vinculin depletion, the cells spread similarly on soft and stiff substrates. In both cases, depleted cells spread less on the 2-MPa rigid substrate than did WT cells (Fig. 3E). This was consistent with the hypothesis that CCs were involved in stabilizing the spread state, and they required α-catenin and vinculin to form.

### Nonmuscle myosin IIB and Tpm2.1 mediate CC

When MDCK cells spread on E-cadherin–coated pillar arrays, they were able to form individual E-cadherin clusters on pillar tips, and phosphorylated myosin light chain (pMLC) was found between E-cadherin clusters (fig. S4A). This resembled fibroblast spreading on fibronectin-coated pillars in that integrins concentrated on pillars, whereas pMLC was in between (*9*). We also observed that treatment with Y-27632, a Rho-associated protein kinase (ROCK) inhibitor, fully abolished CC formation in COS-7 cells (fig. S5B). These results indicated that myosin activity was critical for CC formation.

Previous studies indicated that all three types of nonmuscle myosin II activity were involved in E-cadherin contact dynamics (*27*, *42*) and E-cadherin–based force generation (*8*). However, COS-7 cells lacked nonmuscle myosin IIA and expressed primarily myosin IIB plus a minor fraction of myosin IIC (*33*). Because the CC density was similar in COS-7 and MDCK cells, it was unlikely that myosin IIA was involved in CCs. To determine whether myosin IIB or myosin IIC were involved in CCs, we immunostained COS-7 cell spread on E-cadherin substrata for different myosin II isoforms and observed that myosin IIB immunostaining colocalized with pMLC at the cell edge, where most of the CCs were found (fig. S5C). At a super-resolution level, phosphorylated myosin IIB bipolar minifilaments were observed between two contracting pillars (Fig. 4A), indicating direct involvement of myosin IIB in CC formation. To confirm that myosin IIB powered CC formation, we tested MDCK cells with either myosin IIA or myosin IIB KD (*43*) and observed that both myosin IIA and myosin IIB KD decreased CC formation compared with WT MDCK cells (Fig. 4B). Myosin IIB KD MDCK cells also failed to spread in a rigidity-sensitive manner on E-cadherin and spread significantly less than either control or myosin IIA KD cells (Fig. 4C). It is worth noting that myosin IIB KD results in a more significant reduction of CC generation and less difference in spreading area on pillars with different rigidity compared with myosin IIA KD. These results indicated that both myosin IIA and myosin IIB were involved in CC formation in MDCK cells, while myosin IIB appeared to be more indispensable for CC generation and E-cadherin rigidity sensing. To further confirm whether myosin IIA or myosin IIB was able to power CC formation solely, we knocked down myosin IIB with short hairpin RNA (shRNA) and introduced myosin IIA–green fluorescent protein (GFP) in COS-7 cells at the same time to create myosin IIA– and myosin IIC–positive and myosin IIB–negative COS-7 cells (fig. S5D). We found that these cells had significantly fewer CCs than normal COS-7 cells (fig. S5E),

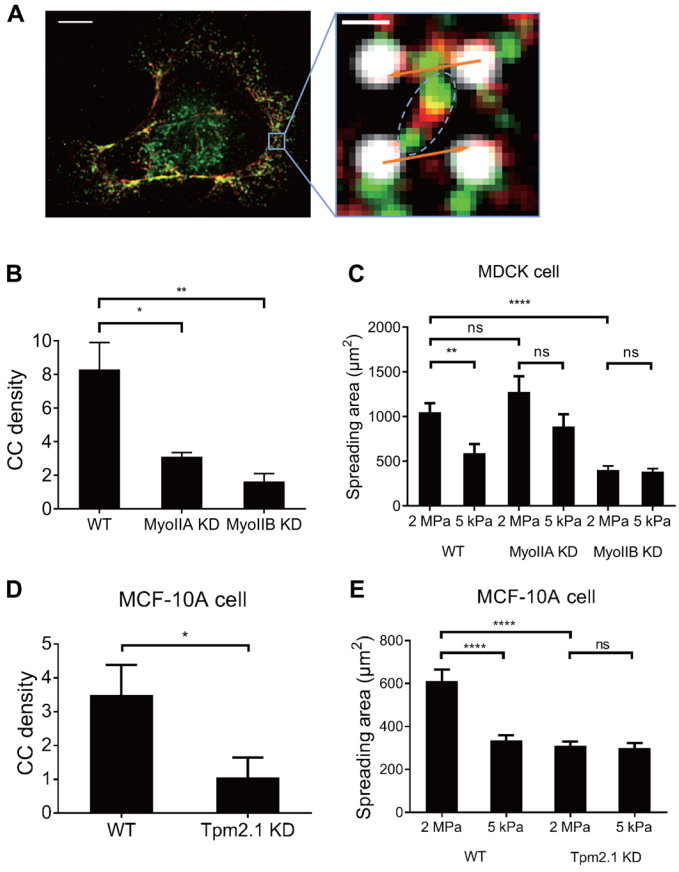


**Fig. 4. Nonmuscle myosin IIB and Tpm2.1 mediate CC formation.** (**A**) Immunostaining of pMLC (green) and myosin IIB heavy chain (red) in COS-7 cell on E-cadherin pillars. Right panel shows phosphorylated myosin IIB minifilament (shown in dashed ellipse) between contracting pillars, deflections of which represented in orange arrows. Scale bars, 5 μm/0.5 μm (left/right panel). (**B**) Myosin IIA KD results in decrease of CC generation (3.12 ± 0.24, $n = 6$ spreading events from four cells in one experiment) compared with WT MDCK cells (8.31 ± 1.60, $n = 9$ spreading events from six cells in four experiments), and myosin IIB KD also results in significant disruption of CC generation compared with WT cells (1.64 ± 0.47, $n = 6$ spreading events from four cells in two experiments). (**C**) KD of myosin IIB in MDCK cells results in similar spreading area on E-cadherin–coated gels with stiffness of 2 MPa (402.3 ± 44.97 μm², $n = 21$ cells from two experiments) or 5 kPa (384.9 ± 33.46 μm², $n = 15$ cells from two experiments), a behavior different from WT cells. KD of myosin IIA also results in similar spreading areas for cells on gels of 2 MPa (1275 ± 175.8 μm², $n = 19$ cells from two experiments) or 5 kPa (889.4 ± 135.7 μm², $n = 11$ cells from two experiments), with nonsignificant increase compared with WT cells. (**D**) Tpm2.1 KD in MCF-10A cells results in decreased CC density (1.06 ± 0.59, $n = 6$ spreading events from four cells in two experiments) compared with WT cells (3.50 ± 0.89, $n = 9$ spreading events from five cells in three experiments). (**E**) MCF-10A cells spread into larger areas on 2-MPa E-cadherin–coated gel (611.7 ± 54.18, $n = 29$ cells from two experiments) than on 5-kPa gel (336.4 ± 22.57, $n = 39$ cells from two experiments), while Tpm2.1KD in MCF-10A cells alters the spreading to be similar on 2 MPa (310.8 ± 19.55, $n = 23$ cells from two experiments) and 5 kPa (300.1 ± 23.43, $n = 34$ cells from two experiments) gels, and spreading area on 2-MPa gels decreases compared with WT cells. *$P < 0.05$; **$P < 0.01$; ****$P < 0.0001$; data are presented as means ± SEM.

confirming that despite involvement of myosin IIA in CC generation, myosin IIB, rather than myosin IIA or myosin IIC, was necessary for CC generation.

Tpm was identified as a major component in integrin contractile units, and cells were incapable of forming contractions or sensing

rigidity when Tpm2.1 protein level was down-regulated (*14*). Previous studies have indicated that several types of Tpm, notably Tpm2.1 and Tpm3.1/3.2, were involved in E-cadherin adhesion integrity (*44*, *45*). We found that Tpm2.1 accumulated in between E-cadherin–coated pillars in newly spread areas where CCs formed in the periphery of COS-7 cells (fig. S6A), which resembled its localization in integrin contractile units (*14*). We also found that pMLC localized to Tpm2.1-rich regions at the cell periphery (fig. S6A) and bridged between two contracting pillars (fig. S6B). To confirm its involvement in CC formation, we knocked down Tpm2.1 in COS-7 cells (see loss of Tpm2.1 staining pattern in KD cells; fig. S6D). Tpm2.1 KD in COS-7 cells resulted in a drastic reduction in the density of CC formation (fig. S6C), indicating that Tpm2.1 played an important role in CC assembly. To further confirm the involvement of Tpm2.1 in CC generation, especially in cells with normal rigidity-sensing behavior, we knocked down Tpm2.1 in MCF-10A cells and observed that KD cells generated fewer CCs (Fig. 4D) and spread similarly on E-cadherin substrates with different rigidity (Fig. 4E), indicating loss of rigidity sensitivity. We also observed that upon Tpm2.1 KD, overall contractions of MCF-10A cells remained unaltered in magnitude compared with WT cells (fig. S6E), indicating that the loss of E-cadherin–mediated rigidity sensitivity upon Tpm2.1 KD is due to the loss of CC, instead of loss of traction force, similar to vinculin KD MDCK cells (Fig. 3, D and E, and fig. S4D). Thus, we suggested that the CC unit between E-cadherin adhesions was distinct molecularly from local contractions of matrix (fig. S7).

### CC regulates myosin IIA–dependent epithelial cell sorting

Previous studies indicated that cell-cell adhesion and cortical tension regulated cell sorting (*46*, *47*), and it was logical to determine whether E-cadherin–mediated mechanotransduction at the cellular level was involved in this process. To test the role of CCs in cell sorting, we first mixed MDCK and COS-7 cells, both capable of forming CCs. Unexpectedly, when MDCK and COS-7 cells (lacking myosin IIA) were mixed and cocultured, the mixed cells exhibited clear segregation, with MDCK cells pushing out COS-7 cells into islands surrounded by MDCK cells (fig. S8A). Previous studies indicated that cell-cell adhesion and cortical tension regulated cell sorting (*46*, *47*), and it was logical to determine whether E-cadherin–mediated mechanotransduction at the cellular level was involved in this process. To test the role of CCs in cell sorting, we first mixed MDCK and COS-7 cells, both capable of forming CCs. Unexpectedly, when MDCK and COS-7 cells (lacking myosin IIA) were mixed and cocultured, the mixed cells exhibited clear segregation, with MDCK cells pushing out COS-7 cells into islands surrounded by MDCK cells (fig. S8A). WT MDCK cells identified myosin IIA–deficient COS-7 cells as stiffness-aberrant cells by CC-dependent stiffness sensing and segregated from them despite their ability of generation CCs. In contrast, CC-deficient α-catenin KD MDCK cells commonly mingled with COS-7 cells and formed islands surrounded by COS-7 cells (fig. S8A). It appeared that α-catenin KD MDCK cells were unable to respond to the lower E-cadherin rigidity expected for the COS-7 cells and were unable to segregate COS-7 cells but rather more randomly mingled with them. Thus, it appeared that CCs were involved in organizing epithelial monolayers by testing myosin IIA–dependent cortical tension of neighboring cells.

To test the generality of this hypothesis, we mixed MDCK cells with or without CCs and myosin IIA KD MDCK cells. Mingling was quantified from the segregation area of myosin IIA–positive cells. We found that WT MDCK cells sorted themselves from myosin IIA KD cells and formed large areas of isolated cell islands. CC-deficient MDCK cells, caused by depletion of either α-catenin, vinculin, or myosin IIB, produced much smaller cell islands and showed greater mingling with myosin IIA KD MDCK cells (Fig. 5A, quantified in Fig. 5B). It is worth noting that vinculin KD cells and myosin IIB KD cells mingled with myosin IIA KD cells at a similar level but less mingled compared with α-catenin KD cells. Thus, it appeared that myosin IIA KD cells were segregated from myosin IIA–positive normal cells that were capable of generating CCs.

We also quantified the time dependence of the segregation using the segregated cell area. WT cells produced a much greater segregated cell area than the myosin IIA KD cells from 24 to 48 hours after mixing, while CC-deficient cells (α-catenin KD cells) showed no change in the level of segregation from myosin IIA KD cells between 24 and 48 hours (fig. S8B, quantified in Fig. 5C). These results indicated that CCs were sensing the cortical tension, which was regulated by myosin IIA, in their neighboring cells, and that sensing was necessary for their segregation from myosin IIA–deficient cells (Fig. 5D).

## DISCUSSION

In this study, we find that an important aspect of mechanosensing in epithelial cells involves paired contractions of E-cadherin adhesions, which correlates with the ability of the cells to sense cadherin rigidity and also to choose neighbors. During CCs, pillar pairs are contracted by a total of 120 to 140 nm for a period of about 20 s irrespective of pillar rigidity over a 19-fold range of rigidity (from ~5 to ~95 kPa). As predicted from previous studies of the proteins in cadherin junctions, α-catenin, vinculin, myosin IIB, and Tpm2.1 are needed for the CC units to form (Fig. 4E). Of the cadherin adhesion complex proteins, α-catenin and vinculin could anchor actin filaments to the adhesions, and Tpm2.1 could stabilize the filaments for myosin IIB contraction. The CCs are distinct from local fibronectin matrix contractions in that myosin IIB, rather than myosin IIA, is necessary for CC generation as well as vinculin and α-catenin. Furthermore, they are distinct from overall radial contractions of E-cadherin–coated pillars in length of deflection and velocity. Although CC pairs form preferentially in newly spread areas of the cell, they continue after cells are spread and are involved in maintenance and dynamics of cell-cell adhesions. Also, we find CC density to be rigidity sensitive because density increases with increasing rigidity in MDCK and MCF-10A cells and decreases with increasing rigidity in COS-7 cells. Furthermore, CC density changes correlate with changes in spread area on different rigidity cadherin surfaces. The organization of epithelial monolayers is highly dependent upon the CCs for both the morphology of the monolayer and the sorting of cells in the monolayer. Thus, it seems that the CCs are important for the formation and maintenance of normal epithelia.

Local contractions between E-cadherin adhesions provide a simple mechanism for testing the rigidity of neighboring cells that is analogous to local matrix, rigidity-sensing contractions, although the details are distinct. Many physiological processes are postulated to involve cadherin adhesion mechanosensing such as convergent extension (*48*) and epithelial tissue movements (*49*). In those cases, changes in monolayer morphology are coupled with continued cell-cell sensing, and this indicates that there are multiple general mechanisms of E-cadherin sensing in tissues (*6*). Recent studies indicate

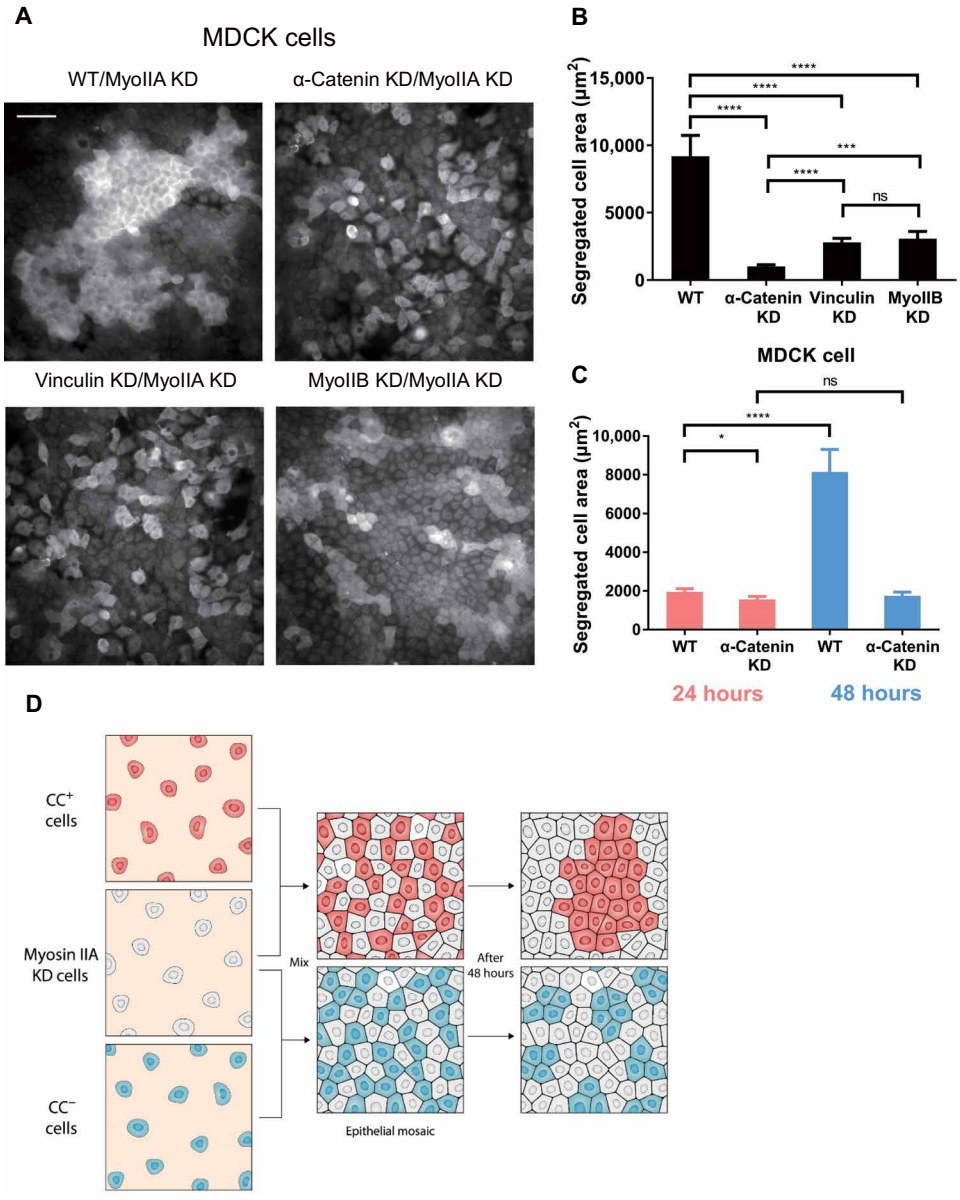


**Fig. 5. CC regulates nonmuscle myosin IIA–dependent MDCK cell sorting.** (**A**) Myosin IIA immunofluorescence indicates populations of MDCK cells (WT, α-catenin KD, vinculin KD, and myosin IIB KD) mixed with myosin IIA KD MDCK cells. Scale bar, 50 μm. (**B**) Quantification of isolated MDCK cell areas after mixing with myosin IIA KD MDCK cells for 48 hours (WT, $n = 30$ areas from three samples; α-catenin KD, $n = 50$ areas from three samples; vinculin KD, $n = 60$ areas from three samples; myosin IIB KD, $n = 50$ areas from three samples). (**C**) Quantification of isolated MDCK cell (WT or α-catenin KD) areas after mixing with myosin IIA KD MDCK cells for 24 hours (in red colored bars, WT, $n = 65$ areas from three samples; α-catenin KD, $n = 50$ areas from three samples) and 48 hours (in blue colored bars, WT, $n = 32$ areas from three samples; α-catenin KD, $n = 55$ areas from three samples). (**D**) Schematic representation of CC-regulated, myosin IIA–sensitive cell sorting. "$CC^+$ cells" refers to cell capable of forming CCs, while "$CC^-$ cells" refers to cell unable to form CCs. *$P < 0.05$; ***$P < 0.001$; ****$P < 0.0001$; data are presented as means ± SEM.

that the rigidity of cadherin-coated surfaces affects cellular responses, indicating that the cells can sense cadherin rigidity (*7*, *8*); however, little is known about how cells use force-generating molecular complexes to test rigidity through cadherin adhesions. The presence of the local contractions provides a simple mechanism for probing cell rigidity, because the force generated by a fixed displacement of an E-cadherin adhesion provides a simple measure of the rigidity of the neighboring cell's cytoskeleton that is coupled to the adhesion. In a general context, although there is only a poor understanding of how contractile force is converted into a signal for rigidity, the many similarities between matrix rigidity sensing and cadherin rigidity sensing make it logical to propose that analogous mechanisms are involved.

In the case of the cell-matrix rigidity sensing, the complex is similar to a sarcomere in terms of the components and the organization. Basically, antiparallel actin filaments cover the 1.5- to 2.5-μm gap between matrix adhesions, and myosin II bipolar filaments contract them at a very slow rate of 2 to 3 nm/s. Similarly, the CCs are driven by myosin II between two adhesions, and the velocity of contractions is 2 to 3 nm/s, which is similar to the rate of matrix

contractions. The major differences are in the type of myosin II, with myosin IIB powering CCs and myosin IIA powering matrix contractions, and in the primary cadherin complex proteins, α-catenin and vinculin, that anchor actin filaments involved in CCs.

In terms of the mechanism of linkage with the actin cytoskeleton, the CCs depend strongly upon α-catenin and vinculin. Both proteins are involved in actin binding to the E-cadherin complex (*10*). KD of α-catenin reduces the number of contraction events. This indicates that α-catenin serves as an important mechanical linker between cadherin adhesions and actomyosin. In addition, α-catenin is generally an important component for force transmission at the cellular level. Similarly, depletion of vinculin causes a marked decrease in the density of CCs. Furthermore, decreasing the vinculin binding affinity of α-catenin also reduces CCs. If vinculin binding is important for stable actin linkages to α-catenin (*37*, *50*), then it is expected that alterations that weaken vinculin binding to α-catenin inhibit CC formation.

The roles of α-catenin and vinculin in CCs extend to their regulatory roles in tissue integrity. α-Catenin has been identified as a tumor suppressor, and its depletion could trigger YAP-1–mediated overgrowth (*51*). Similarly, disruption of myosin-powered contractility also induces YAP-associated contact inhibition failure (*52*). We find that both α-catenin and vinculin KD cause disorder in cell monolayers as previously reported. An unexpected finding is that depletion of vinculin, unlike depletion of α-catenin, does not alter overall force magnitude of cells (figs. S3C and S4D). However, CC density drops, actin organization is altered, and E-cadherin is mislocalized at cell-cell boundaries with vinculin depletion. This highlights the fact that the function of contractile units, instead of overall contractile force, is a major factor in epithelial organization.

Tpm2.1 is critical in matrix rigidity sensing because it helps in the organization of functional actin filaments that support myosin contractions. That it is involved in CCs highlights the similarities between CCs and integrin contractions. Because many transformed cancer cells are deficient in Tpm2.1, there may be an alteration of cadherin rigidity sensing in cancer cells (*14*, *35*). Cancer cells are insensitive to matrix rigidity, and without CCs, they will not be able to test and respond properly to the rigidity of neighboring cells in a tissue. These results further support a critical role for Tpm2.1 in the regulation of tissue integrity and potential cancer suppression through E-cadherin mechanotransduction, in addition to its role in cell-matrix rigidity sensing (*14*).

Classical theories that explain cell sorting describe cell segregation as the result of differential adhesion (*53*) and tension (*46*). Recent studies propose that active forces at cell-cell and cell-substrate interfaces play a major role in cell segregation (*54*). These active forces may be locally regulated by cell-cell rigidity sensitivity. Our findings indicate that an asymmetry in rigidity can fluidize junctions causing movements at cell-cell boundaries, if myosin IIA contractility is deficient. Thus, normal cells will have more stable cell-cell junctions than at normal cell–myosin IIA–null cell junctions, which will aid sorting. However, cells lacking CCs cannot sense their neighbors and then comingle with cells lacking myosin IIA. Among CC-deficient cell types, vinculin KD cells and myosin IIB KD cells share more similarity because only CC generation, instead of overall E-cadherin–dependent mechanotransduction, was disrupted rather than total abolishment of coupling between E-cadherin adhesion complex and actomyosin network, which is likely to be the case in α-catenin KD cells. Such similarity and difference are highlighted by the results that vinculin KD cells and myosin IIB KD cells mingled with myosin IIA KD cells at a lower level than α-catenin KD cells (Fig. 5B), indicating that while CC formation is a key regulator in epithelial cell sorting, total abolishment of E-cadherin–actin coupling could further undermine cell sorting beyond the effect of CC deficiency.

In terms of the relation to surface rigidity, the CCs on rigid pillars will develop stronger contacts than on soft and hence will cause the cell to spread more on rigid pillars. Spreading of the myosin IIA–null COS-7 cells on E-cadherin pillars could be the result of the transformed nature of those cells or a result of the loss of linkage between the sensing system and myosin IIA contractile networks. It is worth mentioning that the mechanical resistance that provides "rigidity" for CC from neighboring cell to test could be dynamic because of the slow rate of contraction. In muscle systems, rapid changes in the rigidity of the attachments do not alter the rate of contraction (*55*). There can be rapid recruitment or activation of molecular components that alter the strength of E-cadherin–actin linkage and actomyosin contractility in response to pulling by neighboring cells. The mechanotransducers related to E-cadherin in cell sorting are potentially critical in long-term epithelial functions, because they can identify weak or dying cells and can facilitate their isolation or removal.

Although myosin activity has been reported as central for junctional E-cadherin recruitment (*23*, *56*), two recent publications have unraveled previously unknown adaptations of cadherin molecular interactions at the nanoscale level that rely (i) on the switch of organization from oligomeric to crystal-like organization depending on cis and trans interactions and affecting the recruitment of additional accessory proteins to the core cadherin-catenin complexes (E-cadherin/β-catenin/α-catenin stoichiometric complexes) (*57*) as well as (ii) on actomyosin activity (*58*). The abovementioned process of E-cadherin cluster strengthening that drives cell-cell adhesions into further maturation shares similarities with CC generation regarding the dependence on adhesion protein recruitment and myosin contractility. The size of these oligomers/clusters (tens of molecules) is compatible with the size of CC described, and they are mechanosensitive and thus may take place downstream or upstream of CC formation in cadherin adhesion mechanosensing. Therefore, we hypothesize that the E-cadherin clusters described above are able to sustain myosin-mediated CCs, which promotes recruitment of additional adhesion proteins to E-cadherin adhesion complexes, and ultimately facilitates the maturation of adherens junctions. In this manner, CCs are potentially important for cis clustering of E-cadherin, and CCs also require trans interaction of E-cadherin to probe the cortical tension of the neighboring cells.

The transient nature of the E-cadherin contraction units is consistent with the transient nature of many cellular mechanosensing processes (*59*). In the MDCK cells, the transient contractions cause a response of more contractions on rigid pillars than on soft pillars, which correlates with greater spread area. There is a need to understand mechanisms of mechanosensory feedback that affect further motility. In cell sorting assays, cells with low myosin IIA levels may naturally sort away from those with high levels because of such downstream responses, implying that the contraction by one cell should elicit a myosin IIA–dependent response from the neighboring cell. CCs provide a simple mechanism for cells to sense the state of their neighbors.

In general, epithelial monolayers undergo a variety of characteristic changes in morphology that involve dynamic physical feedback

between cells. Previous studies indicated that cortical tension is related to myosin IIA activity (*60*). Those motility processes need to be controlled by mechanosensitive signals in order for the proper shape to be reached. In the case of the bending of the *Drosophila* cells, several contraction steps are followed by "consolidation and sensing" steps that determine whether there will be another contraction step (*61*). Thus, it is very important to have the proper mechanosensing signals from measurements of the mechanical aspects of the cell environment such as shape or rigidity. The local CCs provide a means of measuring rigidity that can affect adhesion dynamics and cell boundary motility. Much more is needed to fully understand the motility processes that are affected by the rigidity-sensing CCs.

## MATERIALS AND METHODS

### Cell lines and culture

All MDCK cell lines [American Type Culture Collection (ATCC)] and COS-7 cells (ATCC) were cultured in high-glucose, L-glutamine–containing Dulbecco's modified Eagle's medium (DMEM) with 10% of fetal bovine serum (FBS). For all assays using E-cadherin–coated surfaces, high-glucose, L-glutamine–containing DMEM without FBS and supplemented with penicillin (100 U/ml)/streptomycin (100 μg/ml) was used in experiments. All reagents mentioned above were from Thermo Fisher Scientific. MDCK cell lines (GFP- and mCherry-tagged E-cadherin and α-catenin stable KD cell line), as well as the α-catenin stable KD MDCK cell line, were gifts from W. J. Nelson group (*62*). The vinculin KD MDCK cell line was a gift from S. Yamada group (*63*). Myosin IIA KD and myosin IIB KD MDCK cells were from R.-M.M. group (*43*). COS-7 cell line was from M.P.S. laboratory.

### Plasmids and transfection

Nonmuscle myosin IIB shRNA and vinculin-GFP plasmid were a gift from A. Bershadsky laboratory in Mechanobiology Institute, and vinculin-GFP originated from M. Davidson laboratory in Florida State University. α-Catenin plasmids (WT and L344P mutant) and GFP–E-cadherin plasmids were described earlier (*41*). Tpm2.1 small interfering RNA (siRNA) (Qiagen) was used for KD purpose in COS-7 and MCF-10A cells (*14*).

The Neon Transfection System (Thermo Fisher Scientific) was used for electroporation of MDCK and MCF-10A cells. Lipofectamine 2000 (Thermo Fisher Scientific) was used for chemical transfection of COS-7 cells.

### Preparations of nanopillar arrays and flat gel substrates

We used submicrometer-size pillars for recording and analyzing cell contraction behavior. The pillars were in a square pattern, 600 nm in diameter (*D*), and with three different heights (*L*) of 750, 1500, and 2000 nm. Pillars were made of PDMS (Sylgard 184 Silicone Elastomer Kit), mixed at a ratio of 10:1, spin-coated on silicon molds, and cured at 80°C for 2 hours. For pillars of 600 nm in diameter, bending stiffness was calculated to be ~95 nN/μm for 750-nm tall pillars, ~12 nN/μm for 1500-nm tall pillars, and ~5 nN/μm for 2000-nm tall pillars, and actual stiffnesses were quantified as previously published (*9*). Pillars were patterned in a square grid, with neighboring centroid-to-centroid distance of 1.2 μm [two-dimensional (2D)] or 2.4 μm (4D). Flat PDMS gel surfaces were prepared on glass coverslips with a Sylgard 184 silicone elastomer kit (Dow Corning). PDMS surfaces with a Young's modulus of 2 MPa were made with an elastomer to curing agent ratio of 10:1, and 5-kPa surfaces were made with a ratio of 75:1, as previously published (*64*).

For E-cadherin coating, PDMS films with polymerized pillars were peeled from silicon molds, placed on 12-mm glass-bottom dishes (Iwaki), and treated with $O_2$ plasma for 5 min. Then, they were incubated with anti-human Fc antibody (10 μg/ml; Jackson Research, goat anti-human) in 0.1 M borate buffer (pH 8) at 4°C overnight. For flat PDMS substrates, samples were treated by the same procedure without surface plasma treatment. Coated substrates were washed three times with Dulbecco's phosphate-buffered saline (DPBS), reacted with E-cadherin–Fc chimera protein (10 μg/ml; R&D Systems, diluted in DPBS containing $Mg^{2+}$ and $Ca^{2+}$) for 2 hours in room temperature, and washed three times with DPBS before use.

### Cell spreading assay, drug treatment, and immunostaining

MDCK cells (WT and all KD lines) were trypsinized and replated onto E-cadherin–coated pillar arrays at low density in serum-free medium as mentioned above and incubated at 37°C for 3 hours for cells to properly adhere to pillars before transfer to the microscope for imaging. For spreading assays on PDMS gels, cells were replated onto E-cadherin–coated PDMS gels at low density in serum-free medium and incubated at 37°C for 6 hours before fixation and staining. COS-7 cells were trypsinized and replated onto E-cadherin–coated pillars and imaged immediately since they started to spread in a rapid manner. For Y-27632 (Y0503, Sigma-Aldrich) treatment, COS-7 cells were treated with 10 μM Y-27632 for 2 hours, resuspended with drug-containing serum-free medium, and seeded onto pillar substrates for image acquisition.

For cell immunostaining in general, cells were fixed with 3.7% paraformaldehyde (diluted in DPBS containing $Mg^{2+}$ and $Ca^{2+}$) for 15 min at 37°C, permeabilized with 0.1% Triton X-100 for 10 min at room temperature, and blocked with 1% bovine serum albumin/DPBS solution (blocking buffer) for 1 hour before staining with primary antibody in blocking buffer at 4°C overnight. Samples were washed four times with DPBS before secondary antibody staining in blocking buffer for 1 hour at room temperature and washed four times afterward before 4′,6-diamidino-2-phenylindole (DAPI) staining for 5 min. Phalloidin staining was applied together with secondary antibody incubation for 1 hour.

Primary antibodies used in these experiments are listed as follows: phospho-myosin light chain 2 [$Ser^{19}$, mouse monoclonal antibody (mAb) #3675 and rabbit mAb #3671, Cell Signaling Technology], nonmuscle myosin IIA (M8064, Sigma-Aldrich), nonmuscle myosin IIB (CMII 23, Developmental Studies Hybridoma Bank), nonmuscle myosin IIC heavy chain (PRB-444P, Covance), Tpm2.1 (TM311, Sigma-Aldrich), Tpm3.1/3.2 (ab180813, Abcam), and E-cadherin (610181, BD Biosciences).

### Cell sorting assay

For MDCK cell–COS-7 cell mixture, MDCK cells (WT or α-catenin KD) and COS-7 cells were trypsinized, counted and mixed at a 1:1 ratio, and seeded at a total density of $5.6 \times 10^5$ cells per dish after centrifugation and resuspension. For MDCK cell mixture, myosin IIA–positive MDCK cells (WT, α-catenin KD, vinculin KD, or myosin IIB KD) were mixed with myosin IIA KD MDCK cells at a 1:4 ratio and seeded at a total density of $7 \times 10^5$ cells per dish. Mixed cells were incubated in 12-mm glass-bottom dish (Iwaki) for 48 hours before immunostaining unless otherwise specified.

Myosin IIA was stained as mentioned above in all mixed monolayers to distinguish between MDCK and COS-7 cells or between myosin IIA–positive and myosin IIA–negative MDCK cells. Cell areas with positive myosin IIA immunostaining intensity were thresholded and quantified to indicate the level of sorting segregation between different types of cells. Fluorescence-positive segregated areas below 190 $\mu m^2$ were excluded to avoid dead cell aggregates exhibiting autofluorescence.

### Microscopy imaging and data analysis

Cell spreading on pillars was imaged with a DeltaVision system attached to an Olympus IX71 inverted microscope with 60× water immersion objective or 100× oil immersion objective and Photometrics CoolSNAP HQ2 (charge-coupled device) camera. SoftWoRx (4.10) software was used to control the imaging configuration and recording. Fluorescence images of cells on pillars or PDMS gels were acquired using a spinning-disc confocal microscope (PerkinElmer) attached to an Olympus IX81 inverted microscope. Super-resolution confocal images were acquired using Live-SR (Roper Scientific) module attached to a Nikon Eclipse Ti-E inverted microscope body, controlled by MetaMorph (7.10.1.161), iLas (1.2.0), and Live-SR (1.7.3) software.

Pillar position detection was conducted in ImageJ [National Institutes of Health (NIH)] through tracking plugins designed by F. Margadant. Pillar deflection analysis was conducted through MATLAB (MathWorks).

To identify CC units reflected in pillar movements as paired contractions, we used the method developed in a previous study (*17*). Data files with the position coordinates of cellular pillars (pillars being covered and pulled by cell during imaging) and reference pillars (pillars outside cell area throughout imaging) were imported to a MATLAB program to automatically generate force vector maps for the detected CC units (in green vectors, in contrast to nonpaired pillar deflections in red vectors) and output the number of CC units per frame. Threshold parameters were set by users to identify CC units, including the time threshold, displacement threshold, and pillar spacing. For analysis of each time-lapse image, we fixed the time threshold as 8 s and pillar spacing as 1200 nm and defined the displacement threshold as half of the average $D_{max}$ value calculated from overall pillar deflections of the movie. We also demanded that $D_{max}$ of both pillars occurred within a time window of 5 s to be identified as a paired deflection. Therefore, CC units were identified on freshly contacted pillars with a detection criterion requiring that two or more neighboring pillars were pulled toward each other over the displacement threshold for more than 8 s.

Statistical analysis and graph plotting were generated using Prism (GraphPad Software), and all bar plots were presented as means ± SEM. All data were presented as means ± SEM unless otherwise specified. Analyses of statistical significance levels were performed using Mann-Whitney test.

## SUPPLEMENTARY MATERIALS

Supplementary material for this article is available at https://science.org/doi/10.1126/sciadv.abk0387

View/request a protocol for this paper from *Bio-protocol*.

## REFERENCES AND NOTES


1. V. Vogel, M. Sheetz, Local force and geometry sensing regulate cell functions. *Nat. Rev. Mol. Cell Biol.* **7**, 265–275 (2006).
2. C. M. Lo, H. B. Wang, M. Dembo, Y. L. Wang, Cell movement is guided by the rigidity of the substrate. *Biophys. J.* **79**, 144–152 (2000).
3. R. Sunyer, V. Conte, J. Escribano, A. Elosegui-Artola, A. Labernadie, L. Valon, D. Navajas, J. M. García-Aznar, J. J. Muñoz, P. Roca-Cusachs, X. Trepat, Collective cell durotaxis emerges from long-range intercellular force transmission. *Science* **353**, 1157–1161 (2016).
4. H. B. Wang, M. Dembo, Y. L. Wang, Substrate flexibility regulates growth and apoptosis of normal but not transformed cells. *Am. J. Physiol. Cell Physiol.* **279**, C1345–C1350 (2000).
5. A. J. Engler, S. Sen, H. L. Sweeney, D. E. Discher, Matrix elasticity directs stem cell lineage specification. *Cell* **126**, 677–689 (2006).
6. D. E. Discher, P. Janmey, Y.-L. Wang, Tissue cells feel and respond to the stiffness of their substrate. *Science* **310**, 1139–1143 (2005).
7. C. Collins, A. K. Denisin, B. L. Pruitt, W. J. Nelson, Changes in E-cadherin rigidity sensing regulate cell adhesion. *Proc. Natl. Acad. Sci. U.S.A.* **114**, E5835–E5844 (2017).
8. B. Ladoux, E. Anon, M. Lambert, A. Rabodzey, P. Hersen, A. Buguin, P. Silberzan, R.-M. Mège, Strength dependence of cadherin-mediated adhesions. *Biophys. J.* **98**, 534–542 (2010).
9. S. Ghassemi, G. Meacci, S. Liu, A. A. Gondarenko, A. Mathur, P. Roca-Cusachs, M. P. Sheetz, J. Hone, Cells test substrate rigidity by local contractions on submicrometer pillars. *Proc. Natl. Acad. Sci. U.S.A.* **109**, 5328–5333 (2012).
10. B. Ladoux, W. J. Nelson, J. Yan, R.-M. Mege, The mechanotransduction machinery at work at *adherens* junctions. *Integr. Biol.* **7**, 1109–1119 (2015).
11. M. Takeichi, Dynamic contacts: Rearranging adherens junctions to drive epithelial remodelling. *Nat. Rev. Mol. Cell Biol.* **15**, 397–410 (2014).
12. B. Ladoux, R.-M. Mege, Mechanobiology of collective cell behaviours. *Nat. Rev. Mol. Cell Biol.* **18**, 743–757 (2017).
13. A. Saez, A. Buguin, P. Silberzan, B. Ladoux, Is the mechanical activity of epithelial cells controlled by deformations or forces? *Biophys. J.* **89**, L52–L54 (2005).
14. H. Wolfenson, G. Meacci, S. Liu, M. R. Stachowiak, T. Iskratsch, S. Ghassemi, P. Roca-Cusachs, B. O'Shaughnessy, J. Hone, M. P. Sheetz, Tropomyosin controls sarcomere-like contractions for rigidity sensing and suppressing growth on soft matrices. *Nat. Cell Biol.* **18**, 33–42 (2016).
15. G. Meacci, H. Wolfenson, S. Liu, M. R. Stachowiak, T. Iskratsch, A. Mathur, S. Ghassemi, N. Gauthier, E. Tabdanov, J. Lohner, A. Gondarenko, A. C. Chander, P. Roca-Cusachs, B. O'Shaughnessy, J. Hone, M. P. Sheetz, α-Actinin links extracellular matrix rigidity-sensing contractile units with periodic cell-edge retractions. *Mol. Biol. Cell* **27**, 3471–3479 (2016).
16. B. Yang, Z. Z. Lieu, H. Wolfenson, F. M. Hameed, A. D. Bershadsky, M. P. Sheetz, Mechanosensing controlled directly by tyrosine kinases. *Nano Lett.* **16**, 5951–5961 (2016).
17. M. Saxena, S. Liu, B. Yang, C. Hajal, R. Changede, J. Hu, H. Wolfenson, J. Hone, M. P. Sheetz, EGFR and HER2 activate rigidity sensing only on rigid matrices. *Nat. Mater.* **16**, 775–781 (2017).
18. B. Ladoux, R.-M. Mege, X. Trepat, Front-rear polarization by mechanical cues: From single cells to tissues. *Trends Cell Biol.* **26**, 420–433 (2016).
19. R. Changede, X. Xu, F. Margadant, M. P. Sheetz, Nascent integrin adhesions form on all matrix rigidities after integrin activation. *Dev. Cell* **35**, 614–621 (2015).
20. Y. Wu, P. Kanchanawong, R. Zaidel-Bar, Actin-delimited adhesion-independent clustering of E-cadherin forms the nanoscale building blocks of adherens junctions. *Dev. Cell* **32**, 139–154 (2015).
21. C. M. Niessen, D. Leckband, A. S. Yap, Tissue organization by cadherin adhesion molecules: Dynamic molecular and cellular mechanisms of morphogenetic regulation. *Physiol. Rev.* **91**, 691–731 (2011).
22. D. E. Leckband, J. de Rooij, Cadherin adhesion and mechanotransduction. *Annu. Rev. Cell Dev. Biol.* **30**, 291–315 (2014).
23. R.-M. Mège, N. Ishiyama, Integration of cadherin adhesion and cytoskeleton at *adherens* junctions. *Cold Spring Harb. Perspect. Biol.* **9**, a028738 (2017).
24. T. Lecuit, A. S. Yap, E-cadherin junctions as active mechanical integrators in tissue dynamics. *Nat. Cell Biol.* **17**, 533–539 (2015).
25. S. W. Moore, P. Roca-Cusachs, M. P. Sheetz, Stretchy proteins on stretchy substrates: The important elements of integrin-mediated rigidity sensing. *Dev. Cell* **19**, 194–206 (2010).
26. S. Ebrahim, T. Fujita, B. A. Millis, E. Kozin, X. Ma, S. Kawamoto, M. A. Baird, M. Davidson, S. Yonemura, Y. Hisa, M. A. Conti, R. S. Adelstein, H. Sakaguchi, B. Kachar, NMII forms a contractile transcellular sarcomeric network to regulate apical cell junctions and tissue geometry. *Curr. Biol.* **23**, 731–736 (2013).
27. W. Choi, B. R. Acharya, G. Peyret, M.-A. Fardin, R.-M. Mège, B. Ladoux, A. S. Yap, A. S. Fanning, M. Peifer, Remodeling the zonula adherens in response to tension and the role of afadin in this response. *J. Cell Biol.* **213**, 243–260 (2016).
28. W. Engl, B. Arasi, L. L. Yap, J. P. Thiery, V. Viasnoff, Actin dynamics modulate mechanosensitive immobilization of E-cadherin at adherens junctions. *Nat. Cell Biol.* **16**, 587–594 (2014).
29. A. C. Martin, B. Goldstein, Apical constriction: Themes and variations on a cellular mechanism driving morphogenesis. *Development* **141**, 1987–1998 (2014).

30. A. Ganz, M. Lambert, A. Saez, P. Silberzan, A. Buguin, R.-M. Mège, B. Ladoux, Traction forces exerted through N-cadherin contacts. *Biol. Cell* **98**, 721–730 (2006).
31. M. Lambert, O. Thoumine, J. Brevier, D. Choquet, D. Riveline, R.-M. Mège, Nucleation and growth of cadherin adhesions. *Exp. Cell Res.* **313**, 4025–4040 (2007).
32. R. J. Flannery, J. L. Bruses, N-cadherin induces partial differentiation of cholinergic presynaptic terminals in heterologous cultures of brainstem neurons and CHO cells. *Front. Synaptic Neurosci.* **4**, 6 (2012).
33. J. Bao, S. S. Jana, R. S. Adelstein, Vertebrate nonmuscle myosin II isoforms rescue small interfering RNA-induced defects in COS-7 cell cytokinesis. *J. Biol. Chem.* **280**, 19594–19599 (2005).
34. A. Jasaitis, M. Estevez, J. Heysch, B. Ladoux, S. Dufour, E-cadherin-dependent stimulation of traction force at focal adhesions via the Src and PI3K signaling pathways. *Biophys. J.* **103**, 175–184 (2012).
35. B. Yang, H. Wolfenson, V. Y. Chung, N. Nakazawa, S. Liu, J. Hu, R. Y.-J. Huang, M. P. Sheetz, Stopping transformed cancer cell growth by rigidity sensing. *Nat. Mater.* **19**, 239–250 (2020).
36. B. L. Doss, M. Pan, M. Gupta, G. Grenci, R.-M. Mège, C. T. Lim, M. P. Sheetz, R. Voituriez, B. Ladoux, Cell response to substrate rigidity is regulated by active and passive cytoskeletal stress. *Proc. Natl. Acad. Sci. U.S.A.* **117**, 12817–12825 (2020).
37. S. Yonemura, Y. Wada, T. Watanabe, A. Nagafuchi, M. Shibata, α-Catenin as a tension transducer that induces adherens junction development. *Nat. Cell Biol.* **12**, 533–542 (2010).
38. M. Yao, W. Qiu, R. Liu, A. K. Efremov, P. Cong, R. Seddiki, M. Payre, C. T. Lim, B. Ladoux, R.-M. Mège, J. Yan, Force-dependent conformational switch of α-catenin controls vinculin binding. *Nat. Commun.* **5**, 4525 (2014).
39. H.-J. Choi, S. Pokutta, G. W. Cadwell, A. A. Bobkov, L. A. Bankston, R. C. Liddington, W. I. Weis, αE-catenin is an autoinhibited molecule that coactivates vinculin. *Proc. Natl. Acad. Sci. U.S.A.* **109**, 8576–8581 (2012).
40. Q. le Duc, Q. Shi, I. Blonk, A. Sonnenberg, N. Wang, D. Leckband, J. de Rooij, Vinculin potentiates E-cadherin mechanosensing and is recruited to actin-anchored sites within adherens junctions in a myosin II-dependent manner. *J. Cell Biol.* **189**, 1107–1115 (2010).
41. R. Seddiki, G. H. N. S. Narayana, P.-O. Strale, H. E. Balcioglu, G. Peyret, M. Yao, A. P. le, C. Teck Lim, J. Yan, B. Ladoux, R.-M. Mège, Force-dependent binding of vinculin to α-catenin regulates cell-cell contact stability and collective cell behavior. *Mol. Biol. Cell* **29**, 380–388 (2018).
42. M. Smutny, H. L. Cox, J. M. Leerberg, E. M. Kovacs, M. A. Conti, C. Ferguson, N. A. Hamilton, R. G. Parton, R. S. Adelstein, A. S. Yap, Myosin II isoforms identify distinct functional modules that support integrity of the epithelial zonula adherens. *Nat. Cell Biol.* **12**, 696–702 (2010).
43. M. L. Heuzé, G. H. N. Sankara Narayana, J. D'Alessandro, V. Cellerin, T. Dang, D. S. Williams, J. C. M. van Hest, P. Marcq, R.-M. Mège, B. Ladoux, Myosin II isoforms play distinct roles in *adherens* junction biogenesis. *eLife* **8**, e46599 (2019).
44. H. Shin, D. Kim, D. M. Helfman, Tropomyosin isoform Tpm2.1 regulates collective and amoeboid cell migration and cell aggregation in breast epithelial cells. *Oncotarget* **8**, 95192–95205 (2017).
45. B. J. Caldwell, C. Lucas, A. J. Kee, K. Gaus, P. W. Gunning, E. C. Hardeman, A. S. Yap, G. A. Gomez, Tropomyosin isoforms support actomyosin biogenesis to generate contractile tension at the epithelial zonula *adherens*. *Cytoskeleton* **71**, 663–676 (2014).
46. J.-L. Maitre, H. Berthoumieux, S. F. G. Krens, G. Salbreux, F. Jülicher, E. Paluch, C.-P. Heisenberg, Adhesion functions in cell sorting by mechanically coupling the cortices of adhering cells. *Science* **338**, 253–256 (2012).
47. M. L. Manning, R. A. Foty, M. S. Steinberg, E. M. Schoetz, Coaction of intercellular adhesion and cortical tension specifies tissue surface tension. *Proc. Natl. Acad. Sci. U.S.A.* **107**, 12517–12522 (2010).
48. M. K. L. Han, E. Hoijman, E. Nöel, L. Garric, J. Bakkers, J. de Rooij, αE-catenin-dependent mechanotransduction is essential for proper convergent extension in zebrafish. *Biology Open* **5**, 1461–1472 (2016).
49. D. Cai, S.-C. Chen, M. Prasad, L. He, X. Wang, V. Choesmel-Cadamuro, J. K. Sawyer, G. Danuser, D. J. Montell, Mechanical feedback through E-cadherin promotes direction sensing during collective cell migration. *Cell* **157**, 1146–1159 (2014).
50. C. D. Buckley, J. Tan, K. L. Anderson, D. Hanein, N. Volkmann, W. I. Weis, W. J. Nelson, A. R. Dunn, Cell adhesion. The minimal cadherin-catenin complex binds to actin filaments under force. *Science* **346**, 1254211 (2014).
51. M. R. Silvis, B. T. Kreger, W.-H. Lien, O. Klezovitch, G. M. Rudakova, F. D. Camargo, D. M. Lantz, J. T. Seykora, V. Vasioukhin, α-catenin is a tumor suppressor that controls cell accumulation by regulating the localization and activity of the transcriptional coactivator Yap1. *Sci. Signal.* **4**, ra33 (2011).
52. H. Hirata, M. Samsonov, M. Sokabe, Actomyosin contractility provokes contact inhibition in E-cadherin-ligated keratinocytes. *Sci. Rep.* **7**, 46326 (2017).
53. M. S. Steinberg, Reconstruction of tissues by dissociated cells. Some morphogenetic tissue movements and the sorting out of embryonic cells may have a common explanation. *Science* **141**, 401–408 (1963).
54. L. Balasubramaniam, A. Doostmohammadi, T. B. Saw, G. H. N. S. Narayana, R. Mueller, T. Dang, M. Thomas, S. Gupta, S. Sonam, A. S. Yap, Y. Toyama, R. M. Mège, J. M. Yeomans, B. Ladoux, Investigating the nature of active forces in tissues reveals how contractile cells can form extensile monolayers. *Nat. Mater.* **20**, 1156–1166 (2021).
55. N. Hersch, B. Wolters, G. Dreissen, R. Springer, N. Kirchgeßner, R. Merkel, B. Hoffmann, The constant beat: Cardiomyocytes adapt their forces by equal contraction upon environmental stiffening. *Biol. Open* **2**, 351–361 (2013).
56. G. R. Kale, X. Yang, J.-M. Philippe, M. Mani, P.-F. Lenne, T. Lecuit, Distinct contributions of tensile and shear stress on E-cadherin levels during morphogenesis. *Nat. Commun.* **9**, 5021 (2018).
57. R. B. Troyanovsky, A. P. Sergeeva, I. Indra, C.-S. Chen, R. Kato, L. Shapiro, B. Honig, S. M. Troyanovsky, Sorting of cadherin–catenin-associated proteins into individual clusters. *Proc. Natl. Acad. Sci. U.S.A.* **118**, e2105550118 (2021).
58. R. Chandran, G. Kale, J.-M. Philippe, T. Lecuit, S. Mayor, Distinct actin-dependent nanoscale assemblies underlie the dynamic and hierarchical organization of E-cadherin. *Curr. Biol.* **31**, 1726–1736.e4 (2021).
59. T. Iskratsch, H. Wolfenson, M. P. Sheetz, Appreciating force and shape-the rise of mechanotransduction in cell biology. *Nat. Rev. Mol. Cell Biol.* **15**, 825–833 (2014).
60. N. Taneja, M. R. Bersi, S. M. Baillargeon, A. M. Fenix, J. A. Cooper, R. Ohi, V. Gama, W. D. Merryman, D. T. Burnette, Precise tuning of cortical contractility regulates cell shape during cytokinesis. *Cell Rep.* **31**, 107477 (2020).
61. A. C. Martin, M. Kaschube, E. F. Wieschaus, Pulsed contractions of an actin-myosin network drive apical constriction. *Nature* **457**, 495–499 (2009).
62. W. A. Thomas, C. Boscher, Y.-S. Chu, D. Cuvelier, C. Martinez-Rico, R. Seddiki, J. Heysch, B. Ladoux, J. P. Thiery, R.-M. Mege, S. Dufour, α-Catenin and vinculin cooperate to promote high E-cadherin-based adhesion strength. *J. Biol. Chem.* **288**, 4957–4969 (2013).
63. G. M. Sumida, T. M. Tomita, W. Shih, S. Yamada, Myosin II activity dependent and independent vinculin recruitment to the sites of E-cadherin-mediated cell-cell adhesion. *BMC Cell Biol.* **12**, 48 (2011).
64. M. Prager-Khoutorsky, A. Lichtenstein, R. Krishnan, K. Rajendran, A. Mayo, Z. Kam, B. Geiger, A. D. Bershadsky, Fibroblast polarization is a matrix-rigidity-dependent process controlled by focal adhesion mechanosensing. *Nat. Cell Biol.* **13**, 1457–1465 (2011).


**Acknowledgments:** We thank all the members of the Sheetz, Mège-Ladoux, and Yu laboratories for help, especially F. Margadant, S. Liu, and B. Yang for help in designing ImageJ plugins and MATLAB codes for pillar analysis. We thank the Core Facilities of Mechanobiology Institute, National University of Singapore. **Funding:** Y.-A.Y. was supported by Mechanobiology Institute, National University of Singapore and Ministry of Education, Singapore grants R-714-001-003-271, R-714-000-119-112, R-714-106-004-135, and R-714-105-001-135. E.N. was supported by Mechanobiology Institute, National University of Singapore and Ministry of Education, Singapore. C.F. was supported by Mechanobiology Institute, National University of Singapore and Ministry of Education, Singapore. H.Y. was supported by the Institute of Bioengineering and Bioimaging, Biomedical Research Council, Agency for Science, Technology and Research (A*STAR), A*STAR (project nos. IAF-PP H18/01/a0/014, IAF-PP H18/01/a0/K14, MedCaP-LOA-18-02, and SC19/20-804505-0000); MOE ARC (MOE2017-T2-1-149); IAF (H18/01/a0/017); SMART CAMP; The Institute for Digital Medicine (WisDM); and Mechanobiology Institute of Singapore (R-714-106-004-135) and University Scholars Programme at the National University of Singapore. R.-M.M. was supported by Fondation ARC, Projet International de Coopération Scientifique (PICS) CNRS programmes, France-Singapour exchange grant, National University of Singapore-Université Sorbonne-Paris-Cité (NUS-SPC) exchange grant, and Fondation pour la Recherche Médicale (FRM). B.L. was supported by Mechanobiology Institute, National University of Singapore, le Laboratoire d'Excellence Who Am I? (ANR-11-LABX-0071), the Ligue Contre le Cancer (Equipe labellisée 2019), the Agence Nationale de la Recherche "POLCAM" (ANR-17-CE13-0013), and "MechanoAdipo" (ANR-17-CE13-0012). M.P.S. was supported by NIH grants; NUS grants; Mechanobiology Institute, National University of Singapore; and CPRIT and Welch foundation grants from Texas, United States. This research was supported, in part, by the Singapore Ministry of Education Academic Research Fund Tier 3 (MOE grant no. MOE2016-T3-1-002). **Author contributions:** Y.-A.Y., B.L., and M.P.S. designed the study. Y.-A.Y. and E.N. performed the experiments. G.H.N.S.N. and M.H. prepared the myosin KD MDCK cell lines. H.Y. supervised Y.-A.Y. C.F. and Y.-A.Y. performed cell sorting experiments. Y.-A.Y., B.L., and M.P.S. analyzed the data. Y.-A.Y., R.-M.M., B.L., and M.P.S. wrote and prepared the manuscript. All authors commented on the manuscript. **Competing interests:** The authors declare that they have no competing interests. **Data and materials availability:** All data needed to evaluate the conclusions in the paper are present in the paper and/or the Supplementary Materials.

Submitted 14 July 2021
Accepted 7 December 2021
Published 28 January 2022
10.1126/sciadv.abk0387